SIN-CHN
SCIENTIFIC PRESS PTE.LTD.

Molecular & Cellular Biomechanics 2025, 22(3), 1118.
https://doi.org/10.62617/mcb1118

Article

Application research of improved red tailed eagle algorithm inspired by biomechanics in parameter identification of photovoltaic cells

Zhongming Yu[1,*], Yu Zhang[1], Cheng Guo[1], Yue Sun[2], Xin Dai[2]

[1] Faculty of Electric Power Engineering, Kunming University of Science and Technology, Kunming 650500, China
[2] School of Automation, Chongqing University, Chongqing 400044, China
*** Corresponding author:** Zhongming Yu, zhgmingyu@163.com

CITATION

Yu Z, Zhang Y, Gao C, et al. Application research of improved red tailed eagle algorithm inspired by biomechanics in parameter identification of photovoltaic cells. Molecular & Cellular Biomechanics. 2025; 22(3): 1118. https://doi.org/10.62617/mcb1118

ARTICLE INFO

Received: 16 December 2024
Accepted: 2 January 2025
Available online: 19 February 2025

Abstract: In response to the problems of insufficient accuracy, slow speed, and poor stability in the current parameter identification process of photovoltaic cells, this study designs a parameter identification method based on Improved Red-tailed Hawk (IRTH) algorithm optimization. Firstly, four photovoltaic cell models and one photovoltaic module model are constructed, and corresponding objective functions are established. Secondly, combining Gaussian mutation and cuckoo search ideas, a Gaussian cuckoo mutation mechanism is proposed to reprocess positional information, thereby optimizing the algorithm population and improving solving efficiency. And further analogize photovoltaic cell units as biomaterial units with specific mechanical response characteristics. By studying its current voltage characteristics, the dynamic response of its photoelectric conversion unit under different lighting and load conditions is revealed, similar to the nonlinear and time-dependent characteristics exhibited by biomaterials under external forces. Again, based on the idea of individual extinction in the white whale algorithm, a red-tailed hawk descent mechanism is proposed to improve the convergence speed. The results of the effectiveness test on the proposed IRTH algorithm showed that it converged the fastest and obtained significantly smaller root mean square errors than other optimization algorithms. Finally, the IRTH was further utilized to parameter identification in RTC France photovoltaic cells and photovoltaic modules Photowatt-PWP 201, with an average improvement rate of 79.94%. Therefore, the improved algorithm has better parameter identification effect and higher reliability.

Keywords: photovoltaic cell parameter identification; improved red-tailed hawk algorithm; tangent flight

1. Introduction

Under the “dual carbon” goal, photovoltaic power generation has been greatly promoted [1]. The rapid growth of Photovoltaic Power Generation (PPG) has put forward higher requirements for accurate modeling of the system. In the model of PPG system, accurate identification of parameters is the key to improving system performance and enhancing fault detection capability [2]. The main methods for Parameter Identification (PI) include solving, deterministic methods, and Meta-Heuristic Algorithms (MHA). The solving method only relies on certain key points on the I-V curve to establish a mathematical model, so its identification accuracy is relatively limited. Deterministic methods, such as the least squares method [3], although able to provide higher accuracy results, may easily lead to premature convergence. Since its high feasibility and fast convergence velocity, MHA can simultaneously compensate for the shortcomings of both methods. Therefore, MHA

has been widely used in PI.

Reference [4] proposed an enhanced grey wolf optimizer based on fusion strategy for photovoltaic model identification. This method dynamically adjusted the position update to find a better layout solution on a global scale. Reference [5] introduced the Pelican algorithm simulation for PI. This algorithm had higher accuracy than the above algorithms, however, it still needed further improvement in convergence speed, identification accuracy, and other aspects. Reference [6] introduced Levy flight and local search mechanisms, but there was still a problem of low identification accuracy. Reference [7] used the chaotic seagull optimization algorithm and probabilistic chaos strategy to improve convergence speed, but there was still room for improvement in identification accuracy. Recently, scholars have proposed a new MHA—Red-tailed Hawk (RTH) algorithm [8]. Through experimental analysis, it has been confirmed that the RTH algorithm performs greater than the other 26 MHAs in the vast majority of cases. Reference [9] utilized the RTH optimization algorithm for parameter classification and identification of natural language. However, the identification results obtained were only slightly better than other algorithms. The main reason is that the Levy flight search efficiency of the RTH is low, and it is prone to Fall into Local Optima (FILO), resulting in insufficient convergence speed and identification accuracy.

In summary, although the MHA mentioned above has some applications in system PI, there are still problems with poor identification performance and the tendency to FILO. Hence, this article designs an Improved Red-tailed Hawk (IRTH) algorithm for PI of photovoltaic cells. Firstly, the Gaussian Cuckoo Mutation Mechanism (GCMM) is introduced during the population initialization phase to increase population diversity. Secondly, a tangent flight strategy is introduced during the predation stage to optimize the step size factor and avoid the algorithm being FILO. Moreover, the study analogizes the photoelectric conversion unit to a biomaterial unit with specific mechanical response characteristics. The current voltage response characteristics of photovoltaic cells are highly similar to the mechanical response characteristics of biomaterials under external forces. Biomaterials typically exhibit complex nonlinear and time-dependent behavior under external forces, and their properties dynamically adjust with changes in external conditions; Similarly, the internal structure and physical characteristics of photovoltaic units also result in different current voltage responses under different lighting and load conditions. Through this analogy, we can gain a deeper understanding of the dynamic working mechanism of photovoltaic units, optimize their photoelectric conversion efficiency, and provide new ideas for the design and performance improvement of photovoltaic modules. Finally, based on the concept of the white whale algorithm, a RTH descent mechanism is proposed for position update to improve the convergence velocity of the algorithm. Experiments have shown that compared to other MHAs, the IRTH algorithm exhibits greater advantages in convergence speed, identification accuracy, and reliability.

2. Photovoltaic cell model

It is crucial to construct an accurate Equivalent Circuit (EqC) model for

photovoltaic cells [10]. Reference [11] has modeled the Single Diode Model (SDM) and the Double Diode Model (DDM). On this basis, this article further establishes Three Diode Models (TDM), Four Diode Models (FDM), as well as mathematical models and corresponding objective functions for photovoltaic modules. In the study of photovoltaic cell models, they can be regarded as biomaterial units with specific mechanical response characteristics [12]. Just as biomaterials exhibit different deformation characteristics under external forces, the current and voltage responses of photovoltaic cells also vary due to differences in internal structure and physical properties under the influence of light and load conditions [13]. Therefore, through in-depth analysis of the current voltage characteristics of photovoltaic cells, not only can the efficiency of their photoelectric conversion be grasped, but also their working mechanism can be better understood, which is crucial for optimizing design and improving performance.

2.1. SDM model

SDM is widely used in practical engineering, and its mathematical model expression is:

$$I_{pv} = I_{ph} - I_{sd}\left\{exp\left[\frac{q(I_{pv}R_{se}+U_{pv})}{AKT}\right]-1\right\}-\frac{I_{pv}R_{se}}{R_{sh}} \quad (1)$$

In the formula, I_{pv} and U_{pv} are the current and voltage output by the photovoltaic cell. I_{ph} means the photocurrent. I_{sd} is the reverse saturation current of the photovoltaic tube. q is the amount of electronic charge. A is the constant factor of the diode. K is the Boltzmann constant. T is the operating temperature of the photovoltaic cell. R_{se} is a series resistor. R_{sh} is a parallel resistor. The 5 parameters that need to be recognized are I_{pv}, I_{sd}, A, R_{se}, and R_{sh}.

2.2. DDM

DDM has the impact of composite current and provides a more accurate physical description of the battery. The mathematical formula for DDM is:

$$I_{pv} = I_{ph} - I_{sd1}\left\{exp\left[\frac{q(I_{pv}R_{se}+U_{pv})}{A_1KT}\right]-1\right\}-I_{sd2}\left\{exp\left[\frac{q(I_{pv}R_{se}+U_{pv})}{A_2KT}\right]-1\right\}-\frac{I_{pv}R_{se}}{R_{sh}} \quad (2)$$

The 7 parameters that need to be recognized are I_{pv}, I_{sd1}, I_{sd2}, A_1, A_2, R_{se}, and R_{sh}.

2.3. TDM

This article models TDM. This model takes into account the influence of leakage current. The basic region of a solar photovoltaic cell has a series resistance, described by the resistance of the semiconductor to the substrate. The TDM is given by Equation (3):

$$I_{pv} = I_{ph} - I_{sd1}\left\{exp\left[\frac{q(I_{pv}R_{se}+U_{pv})}{A_1KT}\right]-1\right\}-I_{sd2}\left\{exp\left[\frac{q(I_{pv}R_{se}+U_{pv})}{A_2KT}\right]-1\right\}-I_{sd3}\left\{exp\left[\frac{q(I_{pv}R_{se}+U_{pv})}{A_3KT}\right]-1\right\}-\frac{I_{pv}R_{se}}{R_{sh}} \quad (3)$$

The 9 parameters that need to be identified are I_{pv}, I_{sd1}, I_{sd2}, I_{sd3}, A_1, A_2, A_3, R_{se}, and R_{sh}.

2.4. FDM model

In contrast, the FDM model has the advantages of higher battery accuracy, minimal error between experimental and calculated data, and higher curve fitting accuracy. The EqC for modeling FDM is displayed in **Figure 1**. The expression for FDM is:

$$I_{pv} = I_{ph} - I_{sd1}\left\{exp\left[\frac{q(I_{pv}R_{se}+U_{pv})}{A_1KT}\right]-1\right\} - I_{sd2}\left\{exp\left[\frac{q(I_{pv}R_{se}+U_{pv})}{A_2KT}\right]-1\right\} - I_{sd3}\left\{exp\left[\frac{q(I_{pv}R_{se}+U_{pv})}{A_3KT}\right]-1\right\} - I_{sd4}\left\{exp\left[\frac{q(I_{pv}R_{se}+U_{pv})}{A_4KT}\right]-1\right\} - \frac{I_{pv}R_{se}}{R_{sh}} \quad (4)$$

The 11 parameters that require to be identified are I_{pv}, I_{sd1}, I_{sd2}, I_{sd3}, I_{sd4}, A_1, A_2, A_3, A_4, R_{se}, and R_{sh}.

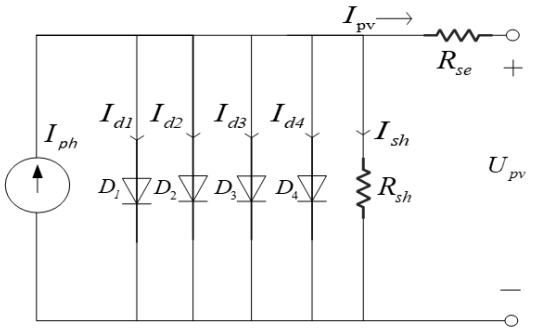

Figure 1. FDM equivalent circuit diagram.

2.5. Photovoltaic module model

Comparing photovoltaic modules to a system composed of multiple biomaterial units with specific mechanical response characteristics can provide a deeper understanding of their overall performance. In nature, different types of biological materials combine to form powerful structural systems not only at the macroscopic level, but also exhibit unique mechanical properties at the microscopic level [14,15]. The interaction between these biomaterials exhibits a synergistic effect, allowing them to flexibly adjust their own response in the face of various external stresses, thereby enhancing overall performance. Similarly, the design of photovoltaic modules also follows this principle, maximizing the unique advantages of each unit and optimizing the photoelectric conversion process through the series and parallel connection of battery cells [16]. This structural integration enables photovoltaic modules to exhibit flexible response capabilities under changing lighting environments and load conditions, thereby significantly improving overall output capability. Just as biomaterials have the ability to adapt to different external forces, the design concept of photovoltaic modules provides a new way of thinking for achieving efficient energy conversion [17]. This analogy not only emphasizes the similarity in design and performance between photovoltaic modules and biomaterials, but also highlights their adaptability in dynamic environments, enabling research to further deepen the understanding of photovoltaic conversion units from the perspective of biomaterials and explore their potential advantages in practical applications. The EqC for modeling it is shown in **Figure 2**. The photovoltaic module model is given by Equation (5):

$$I_{pv} = I_{ph}N_p - I_{sd}N_p\left\{exp\left[\left(I_{pv}R_{se}\left(\frac{N_s}{N_p}\right) + U_{pv}\right)/AN_sV_T\right] - 1\right\} - \frac{I_{pv}R_{se}(N_s/N_p)+U_{pv}}{R_{sh}(N_s/N_p)} \quad (5)$$

N_s means N_s photovoltaic cells in series. N_p represents N_p photovoltaic cells in parallel. There are 5 parameters that require to be recognized, namely I_{pv}, I_{sd}, A, R_{se}, and R_{sh}.

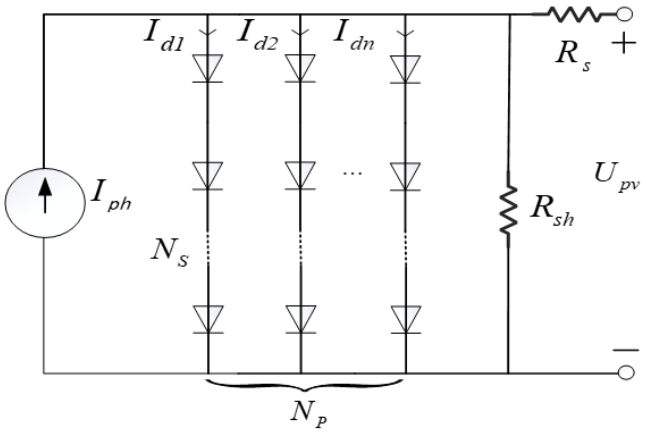

Figure 2. PMM equivalent circuit diagram.

2.6. Establishment of objective function

In the process of establishing the objective function, the study compares the mechanical response characteristics of photoelectric conversion units to biological materials under different loading conditions. Biomaterials typically exhibit complex nonlinear and time-dependent responses, and their performance dynamically adjusts with changes in external conditions. Similarly, the optimization process of the photoelectric conversion unit also needs to fully consider its current and voltage response characteristics under different working states [18,19]. By constructing a reasonable objective function, researchers can ensure that photovoltaic cells can still operate at their optimal state under varying lighting conditions and load influences, thereby effectively improving their photoelectric conversion efficiency. The core goal of photovoltaic cell parameter identification is to accurately determine a set of optimal identification parameter values from actual measured voltage and current data [20]. This process is similar to the evolution of mechanical properties of biomaterials under long-term stress. By optimizing parameters, the simulated values can approach the actual values to the greatest extent possible, reducing the error between the two. Just as biomaterials self-regulate to adapt to external conditions in different environments, photoelectric conversion units also need to demonstrate sensitivity and adaptability to environmental changes in parameter identification. To achieve the goal of ensuring that simulated values can approach actual values to the greatest extent possible, this paper takes root mean square error as the main performance indicator, as shown in Equation (6). Through this method, the PI process is transformed into a problem of finding the optimal value of algorithm error within a specific range, aiming to optimize the prediction accuracy.

$$\delta_{RMSE} = \sqrt{\frac{1}{n}\sum_{i=1}^{n} f\left(U_{i,pv}, I_{i,pv}, x_i\right)^2} \tag{6}$$

n is the number of tests. $f\left(U_{i,pv}, I_{i,pv}, x_i\right)^2$ represents the objective function of each component. x_i is the solution vector of the parameter to be identified.

SDM model objective function and solution vector:

$$\begin{cases} f\left(U_{pv}, I_{pv}, x\right) = I_{ph} - I_{sd}\left\{exp\left[\frac{q\left(I_{pv}R_{se}+U_{pv}\right)}{AKT}\right]-1\right\} - \frac{I_{pv}R_{se}}{R_{sh}} - I_{pv} \\ x = [I_{ph}, I_{sd}, A, R_{se}, R_{sh}] \end{cases} \tag{7}$$

DDM objective function and solution vector:

$$\begin{cases} f\left(U_{pv}, I_{pv}, x\right) = I_{ph} - I_{sd1}\left\{exp\left[\frac{q\left(I_{pv}R_{se}+U_{pv}\right)}{A_1KT}\right]-1\right\} \\ -I_{sd2}\left\{exp\left[\frac{q\left(I_{pv}R_{se}+U_{pv}\right)}{A_2KT}\right]-1\right\} - \frac{I_{pv}R_{se}}{R_{sh}} - I_{pv} \\ x = [I_{ph}, I_{sd1}, I_{sd2}, A_1, A_2, R_{se}, R_{sh}] \end{cases} \tag{8}$$

TDM objective function and solution vector:

$$\begin{cases} f\left(U_{pv}, I_{pv}, x\right) = I_{ph} - I_{sd1}\left\{exp\left[\frac{q\left(I_{pv}R_{se}+U_{pv}\right)}{A_1KT}\right]-1\right\} \\ -I_{sd2}\left\{exp\left[\frac{q\left(I_{pv}R_{se}+U_{pv}\right)}{A_2KT}\right]-1\right\} \\ -I_{sd3}\left\{exp\left[\frac{q\left(I_{pv}R_{se}+U_{pv}\right)}{A_3KT}\right]-1\right\} - \frac{I_{pv}R_{se}}{R_{sh}} - I_{pv} \\ x = [I_{ph}, I_{sd1}, I_{sd2}, I_{sd3}, A_1, A_2, A_3, R_{se}, R_{sh}] \end{cases} \tag{9}$$

FDM objective function and solution vector:

$$\begin{cases} f\left(U_{pv}, I_{pv}, x\right) = I_{ph} - I_{sd1}\left\{exp\left[\frac{q\left(I_{pv}R_{se}+U_{pv}\right)}{A_1KT}\right]-1\right\} \\ -I_{sd2}\left\{exp\left[\frac{q\left(I_{pv}R_{se}+U_{pv}\right)}{A_2KT}\right]-1\right\} \\ -I_{sd3}\left\{exp\left[\frac{q\left(I_{pv}R_{se}+U_{pv}\right)}{A_3KT}\right]-1\right\} \\ -I_{sd4}\left\{exp\left[\frac{q\left(I_{pv}R_{se}+U_{pv}\right)}{A_4KT}\right]-1\right\} - \frac{I_{pv}R_{se}}{R_{sh}} - I_{pv} \\ x = [I_{ph}, I_{sd1}, I_{sd2}, I_{sd3}, I_{sd4}, A_1, A_2, A_3, A_4, R_{se}, R_{sh}] \end{cases} \tag{10}$$

Objective function and solution vector of photovoltaic module model:

$$\begin{cases} f\left(U_{pv}, I_{pv}, x\right) = I_{ph}N_p - I_{sd}N_p\left\{exp\left[\left(I_{pv}R_{se}\left(\frac{N_s}{N_p}\right)+U_{pv}\right)/AN_sV_T\right]-1\right\} \\ -\frac{I_{pv}R_{se}\left(N_s/N_p\right)+U_{pv}}{R_{sh}\left(N_s/N_p\right)} - I_{pv} \\ x = [I_{ph}, I_{sd}, A, R_{se}, R_{sh}] \end{cases} \tag{11}$$

3. RTH optimization algorithm

This article uses the IRTH algorithm to minimize the objective function and

identify the optimal parameter combination for the photovoltaic cell model.

3.1. Standard RTH optimization algorithm

Seydali Ferahtia proposed a novel nature inspired MHA called RTH algorithm in 2023 [21]. As a predator, RTH has 3 stages in the hunting, namely, high-altitude soaring, low-level hovering, and diving hunting. During the high-altitude soaring phase, RTH looks for the search space and decides the range where prey is located. During the low altitude hovering phase, the RTH moves within a chosen area around the prey to select the optimal hunting location. Finally, RTH performs a red-tail swing and hits the target during the diving predation phase. This algorithm simulates the hunting method of RTH to solve optimization problems in the real world.

3.1.1. Soaring high in the sky

RTH flies into the sky, searching for the best position for food supply. Equation (12) represents formula for this stage:

$$X(t) = X_{best} + \left(X_{mean} - X(t-1)\right) \times Levy(d) \times TF(t) \tag{12}$$

$X(t)$ is the position of RTH at t. t is the number of iterations. X_{best} means the best position obtained. X_{mean} is the mean of the position. $Levy(d)$ is the d-dimensional Levy flight formula. $TF(t)$ is a transition factor function that can be calculated based on the equation.

$$\mathrm{TF}(t)=1+\sin\left(2.5+\left(\frac{t}{T_{max}}\right)\right) \tag{13}$$

T_{max} means the maximum iterations.

3.1.2. Low altitude hovering

After choosing the target location in the previous stage, RTH will hover and fly low around the prey. This movement enables it to investigate the optimal position and chance to hit the objective, and deliver a fatal blow to the prey. Its mathematical model is:

$$\begin{gathered} X(t) = X_{best} + \left(x(t) + y(t)\right) \times StepSize(t) \\ StepSize(t) = X(t) - X_{mean} \end{gathered} \tag{14}$$

$StepSize(t)$ indicates the algorithm step size.

3.1.3. Diving prey stage

In this stage, RTH suddenly bends down and attacks prey from the optimal position and timing selected in the previous step during low altitude flight. This stage is very rapid, and its expression is:

$$X(t) = a(t) \times X_{best} + x(t) \times Stepsize1(t) + y(t) \times Stepsize2(t) \tag{15}$$

$a(t)$ is the acceleration coefficient.

3.2. The improved algorithm

3.2.1. The mutation mechanism of gaussian cuckoo bird

To lift the diversity of the algorithm population and lift the convergence velocity,

this study proposes a new mutation mechanism—GCMM—by combining Gaussian Mutation (GM) and Cuckoo Search (CS) in the initialization population stage of the RTH algorithm.

(1) Gaussian mutation

GM uses random numbers that follow a normal distribution to act on the previous location vector, generating new positions and ensuring that mutation activity occurs within a controllable and focused area, resulting in superior results [22]. The GM density formula is:

$$f(x) = \frac{1}{\sqrt{2\pi}\sigma} exp\left(-\frac{(x-\mu)^2}{2\sigma^2}\right) \tag{16}$$

μ denotes the mean or expected value of the distribution. σ means the standard deviation. μ and σ are 0 and 1. The position difference and Gaussian Distribution (GD) operator are applied to design a unique GM operator. The specific expression of this operator is:

$$O = G(\xi) \times \left(X^D_{rand1} - X^D_{rand2}\right) \tag{17}$$

$G(\xi)$ is a GD shaped by the probability density in Equation (16), where $\xi \in [0, 1]$. X^D_{rand1} and X^D_{rand2} are the position of two randomly chosen eagles in the population.

(2) Cuckoo search

CS is a MHA that simulates the parasitic brooding and movement behaviors of cuckoo [23]. The Position Vector (PV) of dimensional data can be randomly mutated through parasitic strategies. The mutated PV keeps the superior features of the previous position. The judgment is expressed as follows:

$$k = Judge^D > \theta \tag{18}$$

$Judge^D$ is a D-dimensional random array. θ is an operator that determines whether to discard the present bird's nest. k refers to the result of comparing each $Judge^D$ dimension with θ, used to determine which data dimension to mutate. The scheme for random movement of cuckoos is:

$$C = k \times Levy(d) \tag{19}$$

C corresponds to the CS operator, and k decides which vector dimension needs to undergo a mutation.

(3) Gaussian cuckoo mutation synthesis

A new mutation mechanism, GCMM, is synthesized using GM and CS ideas and introduced into the original RTH algorithm. GM uses normally distributed random numbers to perturb the position vectors of individuals to generate new positions, ensuring that the mutation activity takes place in a controlled and concentrated area to produce superior results [24]. CS simulates the parasitic breeding behaviour of cuckoos by mutating the PVs of the dimensional data through a stochastic strategy that maintains the superior characteristics of the previous position [25]. The specific steps are:

The first step is to initialize the population, including the size N of the population and the iteration T, etc;

The second step is to randomly select two search agents from the population after

RTH is executed normally, and based on the above two mechanisms, cause a mutation in the differences between the two agents;

The next step is to add the current search position and gain a novel PV;

The final step is comparing the old and new PVs and maintain a good PV. The calculation is:

$$X_{new} = X_{raw} + O \times C$$
$$X(t+1) = \begin{cases} X_{new} & if \ F(X_{new}) < F(X_{raw}) \\ X_{raw} & else \end{cases} \quad (20)$$

X_{raw} denotes the search outcomes of the conventional RTH. X_{new} is the novel position after mutation. $F(X_{raw})$ and $F(X_{new})$ are their fitness functions. O is the GM operator mentioned above, each operator containing d dimensions. C is the CS operator.

Overall, utilizing this mechanism to reprocess location information not only increases population diversity but also improves solving efficiency. The optimized algorithm does not make the previous algorithm's framework more complex.

3.2.2. Tangent flight

The Levy flight used in the original RTH algorithm is a unique random walk model used to characterize movement patterns with long tail distribution characteristics. In terms of PI of photovoltaic cells, Levy's flight process has low search efficiency and is prone to being FILO.

Figure 3 is a random walk graph of Levy flight simulated 1000 times. The multiple iterations at the initial point (0, 0) of the wandering coordinates show that the algorithm's search range is limited to a small area in the early stages of iteration, and cannot effectively cover potential important areas. In addition, the high degree of randomness and narrow step size range also result in repeated searches of the already searched area, leading to local optima.

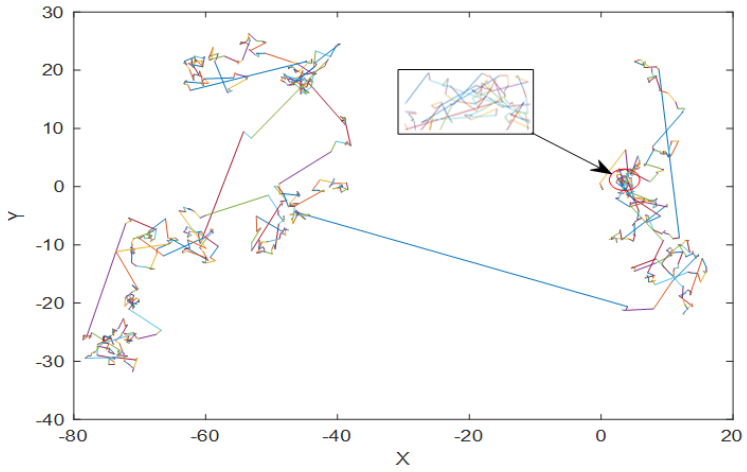

Figure 3. Levy flight random walk diagram.

When the iteration reaches its end (as shown in the left half of **Figure 3**), although the narrow step interval still limits the range of stride changes, the search span at this time is significantly larger than at the beginning of the iteration, leading to the problem of excessive search distance. This "small first, big later" search pattern may not only reduce search efficiency, but also cause the algorithm to miss the optimum, ultimately

leading to the search process being FILO.

Therefore, in response to the characteristic of Levy flight, to avoid the RTH being FILO during the dive hunting phase and improve the convergence speed, a Tangent Search Algorithm (TSA) is introduced during the dive hunting phase of RTH [26]. TSA is introduced in the predation phase of the RTH algorithm, using a tangent function based model to guide the current solution in a more optimal direction. The properties of the tangent function are used to combine global and local search to optimise the step size and improve the search efficiency and accuracy of the algorithm. It adopts a model built on tangent functions to guide the current solution to a more optimum. The specific implementation steps are as follows:

The given optimization algorithm position update formula:

$$X^{t+1} = X^t + step \times w \tag{21}$$

The $step$ is the algorithm stride. w is the direction of movement.

Due to the crucial role of step size in algorithm optimization, a larger step size aids to explore a wider solution space, while a smaller one facilitates finer search. This article introduces the tangent function to obtain a search equation that combines global and local walks, as calculated in Equation (22):

$$X^{t+1} = X^t + step \times tan(\theta) \tag{22}$$

Note: $step$ is represented by $Stepsize(t)$ in this article.

Finally, the expression for the optimal position after introducing tangent flight can be further obtained:

$$X(t) = a(t) \times X_{best} + x(t)Stepsize1(t)\, tan(\theta) + y(t)Stepsize2(t)\, tan(\theta) \tag{23}$$

$a(t)$ is the acceleration coefficient.

$$\begin{aligned} Stepsize1(t) &= X(t) - TF(t) \times X_{mean} \\ Stepsize2(t) &= G(t)X(t) - TF(t) \times X_{best} \end{aligned} \tag{24}$$

$G(t)$ is the gravity effect, which is used to reduce excessive search space.

In addition, the values of $a(t)$ and $G(t)$ can be simplified as follows:

$$a(t) = sin^2\left(2.5 - \frac{t}{T_{max}}\right) \tag{25}$$

As $a(t)$ is a monotonically increasing function, the acceleration of RTH grows with the iterations, thereby improving the convergence speed.

$$G(t) = 2 \times \left(1 - \frac{t}{T_{max}}\right) \tag{26}$$

Due to $G(t)$ being a monotonically decreasing function, the gravity effect of RTH decreases with increasing iteration times, thereby also improving convergence speed.

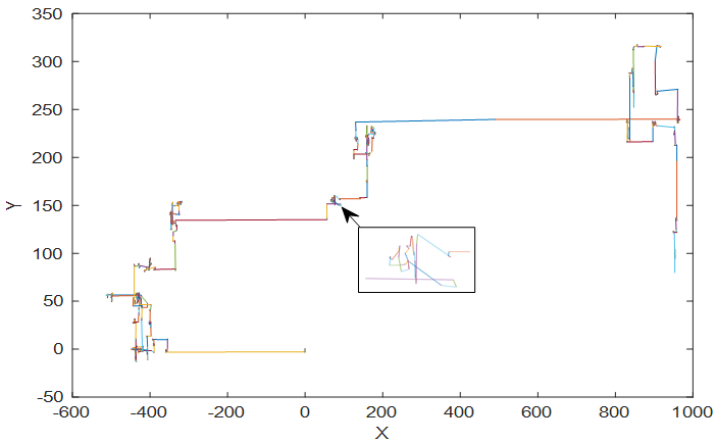

Figure 4. Tangential flight random walk diagram.

Figure 4 shows a tangent flight random walk graph. Compared to **Figure 3**, at point (0, 0), tangent flight does not waste time on small-scale repeated random exploration. The more complex parts in the figure (such as the majority) are clearly simpler than Levy's flight trajectory, overcoming the problem of low search efficiency caused by Levy's high randomness in flight. In addition, compared to the coordinate dimensions in the figure, the search distance of tangent flight is farther than that of Levy flight, thus overcoming the problem of Levy flight having a too small search distance. When the tangent flight iteration reaches its end (as shown in the right half of **Figure 4**), the search distance decreases significantly compared to the initial stage of the iteration, forming a "large first, then small" search pattern. This improves search accuracy and solves the problem of Levy's long search distance in the later stages of flight. By introducing TSA, the algorithm can avoid being FILO, allowing for a wider range of searches and providing more opportunities for RTH to hunt, thereby improving the identification accuracy of the algorithm.

In summary, by introducing tangent flight instead of Levy flight in the IRTH algorithm to optimize the step size factor of the algorithm's predation stage, the shortcomings of Levy flight search distance being too large or too small are compensated for, and the convergence speed and identification accuracy are accelerated.

3.2.3. RTH falling mechanism

To optimize the objective function results and improve the overall performance, the paper constructs an RTH falling mechanism. The probability of RTH falling from individuals in the population is selected as a subjective hypothesis. By establishing an RTH falling mechanism, the optimal results of previous iterations are sorted. By utilizing the probability of RTH falling for position update, the convergence speed is improved. The construction process of the mechanism is:

Firstly, based on the migration and foraging process of white whales in the white whale algorithm [15], the following RTH descent mechanism is constructed to achieve adaptive parameter adjustment of the step size factor.

$$P_f = P_d - \frac{P_l T}{T_{max}} \tag{27}$$

P_f is the probability of RTH falling, and in the objective law of survival at the initial

moment of RTH, the probability of RTH falling is about 0.1. P_d is the initial probability of RTH falling. P_l is the final probability of RTH falling. T is the current iteration count.

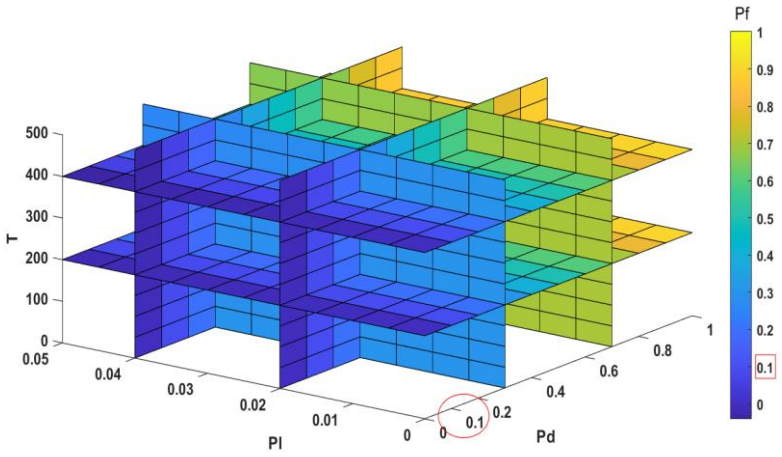

Figure 5. Visual spatial analysis diagram of falling mechanism.

The probability of RTH falling mentioned above, P_f, is 0.1. By visualizing the spatial color gamut analysis of the falling mechanism is shown in **Figure 5**, the value of P_d can be obtained as 0.1, which is used as a subjective assumption to simulate small changes in the population. The value of P_l is selected as 0.05, from which the final probability of RTH falling can be obtained. This probability describes the degree of risk of RTH approaching the food source during the optimization process.

When the RTH is transferred to another location or shot down, its position and the step size of its fall are utilized to determine the updated position:

$$X_{step} = (u_b - l_b)\, exp\left(-C_2 \times \frac{T}{T_{max}}\right) \tag{28}$$

C_2 is the step size factor related to the probability of RTH fall and population size, and u_b and l_b are the upper and lower bounds of the variable X_{step}.

$$C_2 = 2P_f \times n \tag{29}$$

The n is the population size.

$$X_i^{t+1} = r_1 X_i^t - r_2 X_r^t + r_3 X_{step} \tag{30}$$

r_1, r_2, and r_3 are random numbers between (0, 1). X_i is the position of the i-th RTH. X_r is the current position of the r-th RTH. Meanwhile, the study introduces adaptive mechanisms to dynamically adjust the use of optimisation strategies to reduce the computational overhead of the algorithms in systems with limited computational resources. The core idea of the adaptive mechanism is to decide whether to activate a specific optimisation mechanism based on the complexity of the problem and the current search state. First, the problem complexity is assessed, which is achieved by analysing the dimensionality of the objective function, the size of the search space and the historical optimisation difficulty of the problem. Second, the current search state is monitored, including population diversity, the quality of the current best solution, and the speed of search progress. In each iteration of the algorithm, based on the current search state and problem complexity, the adaptive mechanism will

dynamically adjust the weights or parameters of the above optimisation mechanisms. For example, at the beginning of the search, the weight of the Gaussian cuckoo mutation is increased to increase the population diversity; while at the approach of convergence, the weight of the RTH descent mechanism is increased to accelerate the convergence speed.

In summary, by establishing an RTH drop mechanism, it is possible to rank the optimal results of previous iterations and use the RTH drop mechanism for position updates, thereby lifting the convergence velocity. **Figure 6** shows the flowchart of the improved RTH. The IRTH algorithm firstly randomly initialises the location of a flock of eagles in the search space and evaluates the fitness of each eagle using an objective function. Secondly, GCMM is applied to increase the population diversity and the iterative step size of the algorithm is optimised using TSA without avoiding local last. On this basis, RTHFM is used to improve the convergence speed of the algorithm and the descent strategy is dynamically adjusted by an adaptive mechanism. When the stopping condition is satisfied, the optimal result is output.

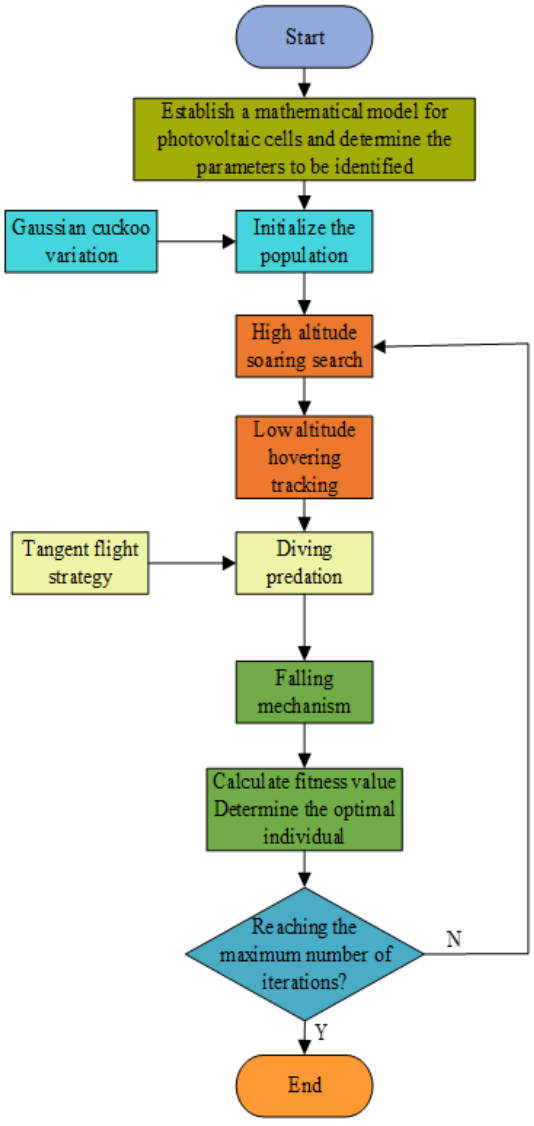

Figure 6. IRTH flow chart.

3.3. Effectiveness testing

To verify that the IRTH algorithm has better optimization results compared to other algorithms, comparative experiments are conducted on six standard test functions for efficient optimization algorithms in the past two years: RTH algorithm, frost ice optimization algorithm [16], snow melting optimization algorithm [17], Pelican optimization algorithm, and Harris Eagle optimization algorithm. The test results are exhibited in **Figure 7a–f**. IRTH achieves a 100% optimization effect among 6 test functions, with the search for the optimal value being even better. In the F_1, F_2, and F_3 functions, when the four algorithms cannot converge and FILO, IRTH successfully seeks optimization with a much faster convergence velocity than others. In the F_4, all other algorithms fail to optimize, and IRTH avoid derivative convergence and escaped local optima. In the convergence curve of the F_5, when all other algorithms have poor optimization results and cannot converge, the IRTH algorithm can still achieve the optimization goal. In the F_6, the convergence speed of the IRTH is significantly faster than others. Overall, the IRTH algorithm exhibits better convergence compared to other algorithms.

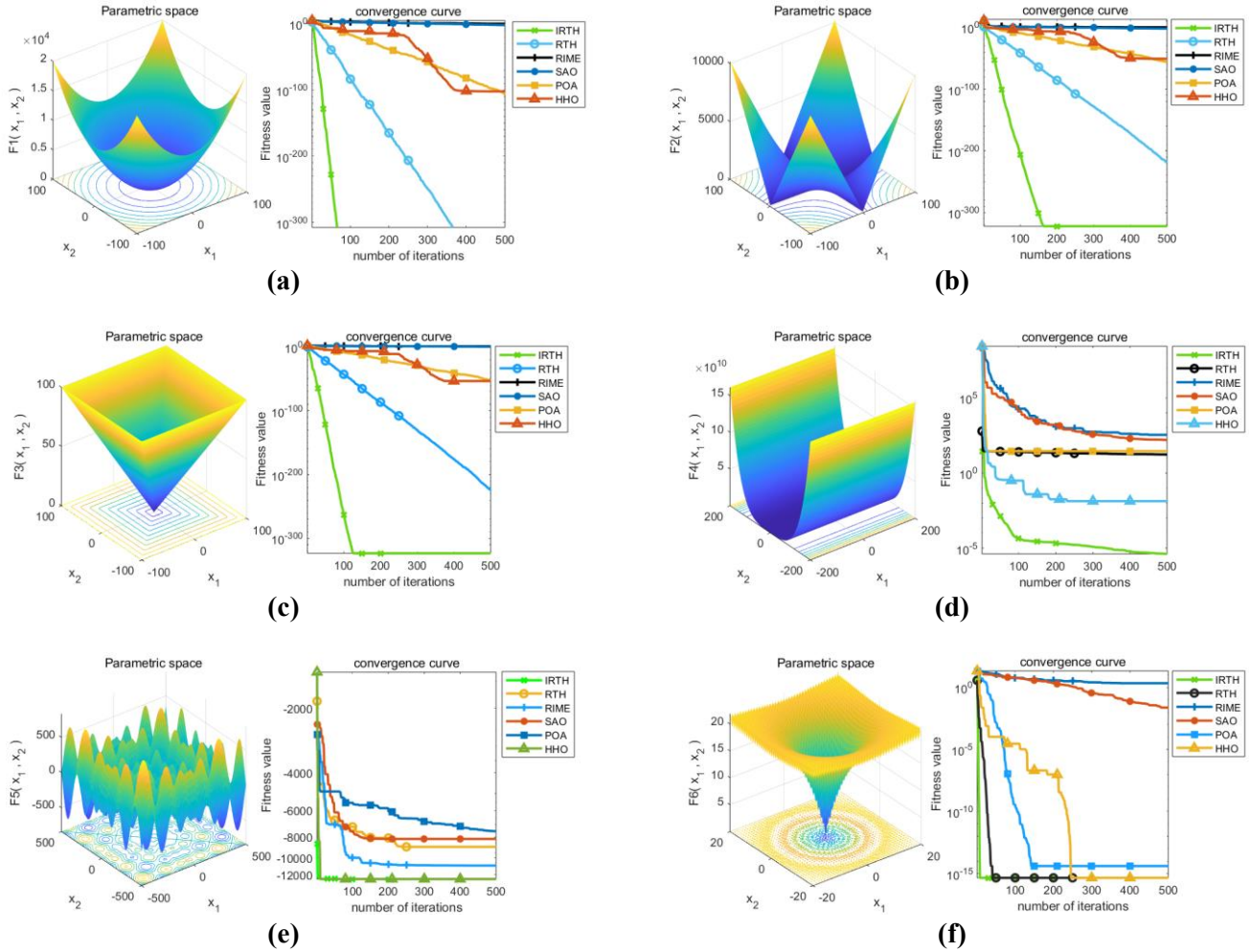

Figure 7. Test functions and convergence curves. **(a)** F_1 test function and convergence curve; **(b)** F_2 test function and convergence curve; **(c)** F_3 test function and convergence curve; **(d)** F_4 test function and convergence curve; **(e)** F_5 function and convergence curve; **(f)** F_6 function and convergence curve.

4. Photovoltaic parameter identification using IRTH algorithm

Table 1. Parameter identification result.

Model	Function	$I_{ph}(A)$	$I_{sd}(\mu A)$	$R_{se}(\Omega)$	$R_{sh}(\Omega)$	A_1	δ_{best}	δ_{mean}
SDM	IRTH	0.7608	3.2332×10^{-7}	0.0364	53.7343	1.4813	0.00098602	0.00098648
	RTH	0.7608	3.2103×10^{-7}	0.0364	53.5734	1.4806	0.00098612	0.0013
	RIME	0.7604	4.4899×10^{-7}	0.0344	48.8068	1.5158	0.0019	0.0068
	SAO	0.7606	4.6194×10^{-7}	0.0349	66.4177	1.5181	0.0012	0.0018
	POA	0.7612	6.4969×10^{-7}	0.0332	72.6135	1.5551	0.0017	0.0024
	HHO	0.7407	6.9977×10^{-7}	0.0334	43.0378	1.5691	0.0197	0.0559
DDM	IRTH	0.7608	2.6007×10^{-7}	0.0366	54.6033	1.4633	0.00098385	0.0011
	RTH	0.7608	1.4188×10^{-8}	0.0363	53.4787	1.4684	0.00098836	0.0012
	RIME	0.7618	4.5022×10^{-7}	0.0342	64.4678	1.5283	0.0019	0.0031
	SAO	0.7601	7.5418×10^{-7}	0.0369	67.3454	1.9313	0.0011	0.0016
	POA	0.7613	2.8542×10^{-7}	0.0358	49.5450	1.4787	0.0011	0.0030
	HHO	0.7573	4.5180×10^{-7}	0.0324	69.3659	1.5193	0.0041	0.0151
TDM	IRTH	0.7608	7.4003×10^{-7}	0.0369	55.8722	1.9864	0.00098417	0.0011
	RTH	0.7610	6.1946×10^{-11}	0.0362	54.3720	1.9998	0.0010	0.0012
	RIME	0.7624	3.7897×10^{-7}	0.0360	99.9886	1.5050	0.0037	0.0056
	SAO	0.7609	2.3045×10^{-9}	0.0315	97.7162	1.8698	0.0024	0.0029
	POA	0.7600	2.8936×10^{-8}	0.0358	100	1.4708	0.0024	0.0039
	HHO	0.7598	9.0546×10^{-7}	0.0156	30.0934	1.7326	0.0145	0.0304
FDM	IRTH	0.7608	1.1730×10^{-7}	0.0370	56.6225	1.6540	0.00098573	0.0011
	RTH	0.7608	8.2140×10^{-7}	0.0369	55.6583	1.9987	0.0010	0.0013
	RIME	0.7618	7.7506×10^{-7}	0.0340	58.6837	1.9726	0.0025	0.0066
	SAO	0.7609	9.0411×10^{-8}	0.0379	59.4887	1.3799	0.0011	0.0027
	POA	0.7615	6.4365×10^{-7}	0.0297	80.1601	1.7914	0.0036	0.0049
	HHO	0.7512	4.2270×10^{-7}	0.0126	42.8975	1.6323	0.0224	0.0334
PMM	IRTH	0.2060	7.4894×10^{-7}	1.9893	1.8597×10^{3}	16.3070	0.0024	0.0035
	RTH	0.2069	9.9398×10^{-7}	1.9369	1.5356×10^{3}	16.6839	0.0032	0.0050
	RIME	0.2091	3.5128×10^{-5}	0.8074	2000	23.5426	0.0175	0.0197
	SAO	0.2075	5.7870×10^{-6}	1.4788	1.9999×10^{3}	19.4912	0.0090	0.0147
	POA	0.2084	4.2326×10^{-6}	1.5323	1.0942×10^{3}	18.9358	0.0090	0.0145
	HHO	0.2099	5.0000×10^{-5}	1.0841	1.8589×10^{3}	24.5504	0.0301	0.0460

Note: δ_{best} identifies the optimal value. δ_{mean} is the average value for identification.

IRTH has been applied to photovoltaic cell models and compared with efficient algorithms in PI accuracy, convergence speed, and stability in the past two years. DDM is RTC France photovoltaic cell. Photowatt-PWP 201 is selected as the photovoltaic module.

Under standard conditions (temperature of 33 °C, 1000 W/m^2 light intensity), the measured voltage and current data are inputted into the identification model and simulated on the simulation platform. To lower down the effect of random errors on

the accuracy, the maximum iterations for the algorithm are set to 500, and each algorithm is independently run 15 times.

The SDM identification results in **Table 1** show that in 15 independent tests, the optimal and average error values optimized using IRTH are 0.00098602 and 0.00098648. Although RTH achieves similar results at the optimal value, IRTH performs better than other algorithms in average metrics. This indicates that the stability of IRTH is relatively better while ensuring the accuracy of PI. **Figure 8** is that the convergence speed of IRTH during PI is better than other algorithms, and the final optimum identified is significantly smaller than others. The I-V and P-V curves of SDM are exhibited in **Figure 9**. The simulated values identified using IRTH have a very high degree of fit with the actual values.

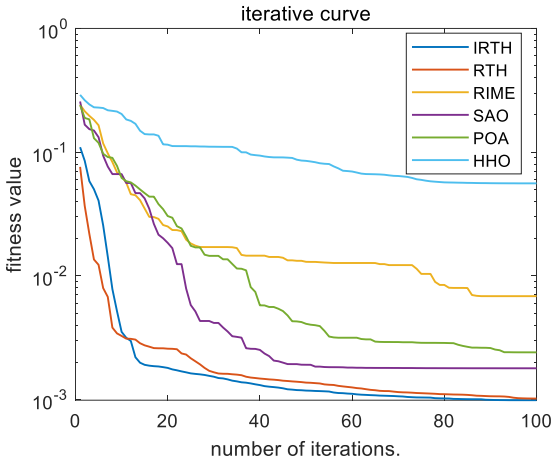

Figure 8. Parameter identification of SDM.

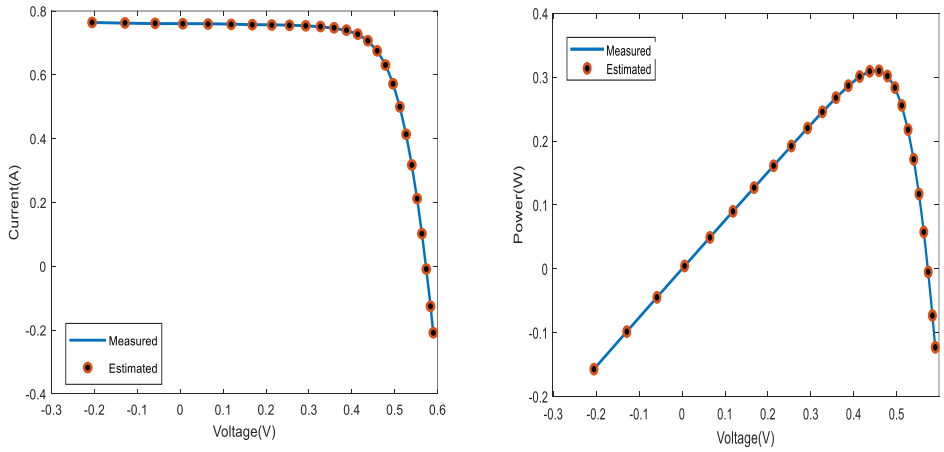

(a) **(b)**

Figure 9. Comparative chart of SDM: **(a)** I-V characteristics; **(b)** P-V characteristics.

Figure 10 shows the convergence diagram of the DDM PI. The DDM identification results in **Table 1** and the DDM current voltage curve presented in **Figure 11** indicate that the simulated values are highly consistent with the electrical characteristics of the battery. This further proves the accuracy and reliability of the IRTH algorithm in identifying current values. Overall, the IRTH algorithm has demonstrated significant advantages and accuracy in identifying parameters for DDM

models.

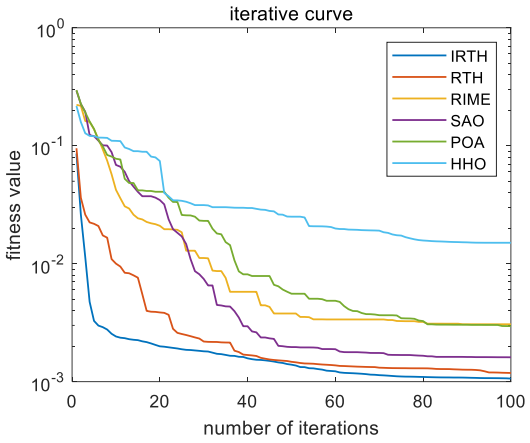

Figure 10. Parameter identification of DDM.

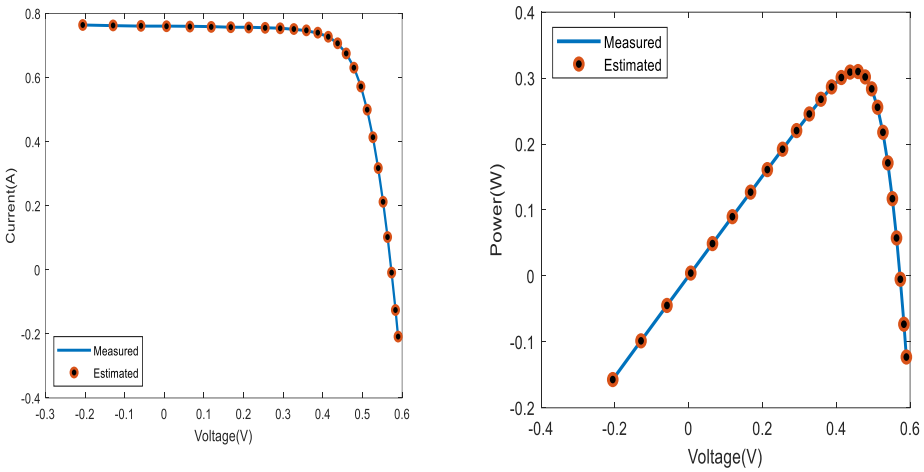

(a) **(b)**

Figure 11. Data comparison chart of DDM: **(a)** I-V characteristics; **(b)** P-V characteristics.

The TDM identification results in **Table 1** show that IRTH performs well in identifying TDM models, and the optimal and average error values optimized using IRTH are superior to other algorithms. This indicates that IRTH exhibits higher excellence when facing more complex and precise systems. **Figure 12** shows the convergence diagram of TDM PI. In the process of identifying parameters, the convergence speed of IRTH is very fast, far exceeding other optimization algorithms. This further demonstrates the superiority of IRTH. The current voltage curve of TDM in **Figure 13** shows that the current and power are extremely consistent with the actual data. This result confirms that IRTH has higher accuracy in TDM identification than other algorithms.

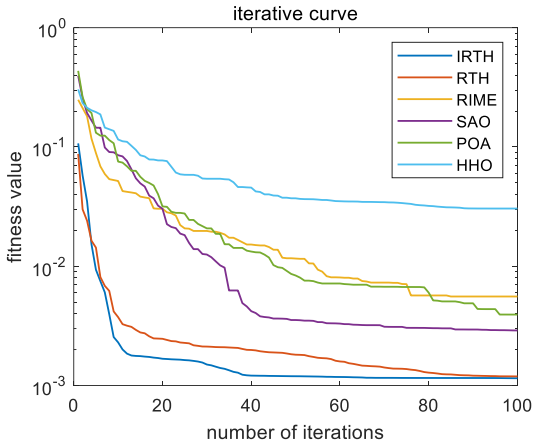

Figure 12. Parameter identification of TDM.

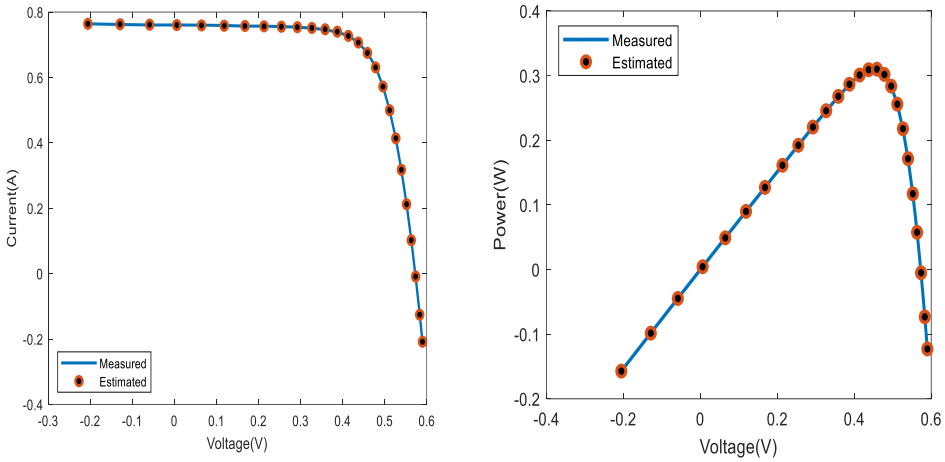

(a) **(b)**

Figure 13. Comparative data of TDM. **(a)** I-V characteristics; **(b)** P-V characteristics.

In the FDM identification results of **Table 1**, as the model becomes more complex, the identification errors of other algorithms are gradually increasing, demonstrating the high stability of IRTH in dealing with complex systems. **Figure 14** illustrates the convergence diagram of the FDM PI. During the parameter identification process, the convergence speed of IRTH is notably rapid, significantly outperforming other optimization algorithms. This further highlights the superiority of IRTH. The current-voltage curve of the FDM in **Figure 15** demonstrates that both the current and power are in excellent agreement with the actual data.

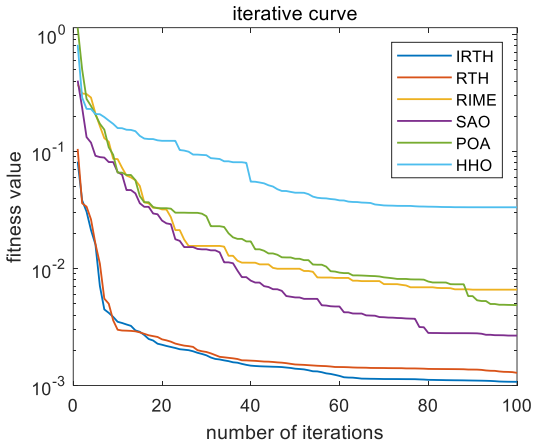

Figure 14. Parameter identification of FDM.

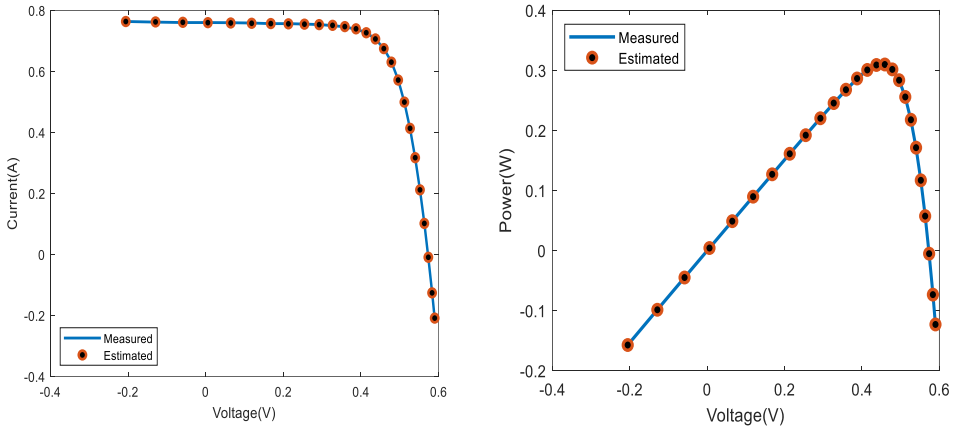

Figure 15. Data comparison chart of FDM. **(a)** I-V characteristics; **(b)** P-V characteristics.

The identification results of photovoltaic modules in **Table 1** indicate that IRTH performs the best in photovoltaic module identification. The optimal and average error values optimized using IRTH are 0.0024 and 0.0035. Compared with the δ_{best} values identified by other algorithms, the δ_{best} value identified by IRTH is smaller. Compared with the δ_{mean} values of other algorithms, the improvement rate of IRTH is 82.56%.

In **Figure16**, the convergence speed of IRTH during the PI process is similar to RTH and faster than other algorithms before the 40th iteration. After the 40th iteration, the convergence speed of IRTH is significantly faster than RTH, and the final identified optimum is significantly smaller than all algorithms. In **Figure 17**, the simulated I-V and P-V curves are highly fitted to the measured values. This high level of accuracy is crucial for further research and analysis of photovoltaic cell fault diagnosis in the future.

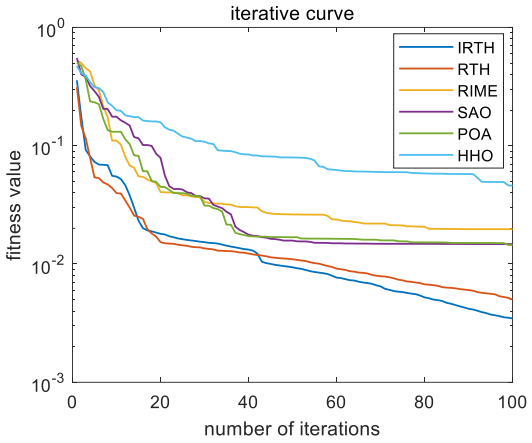

Figure 16. PMM equivalent circuit diagram.

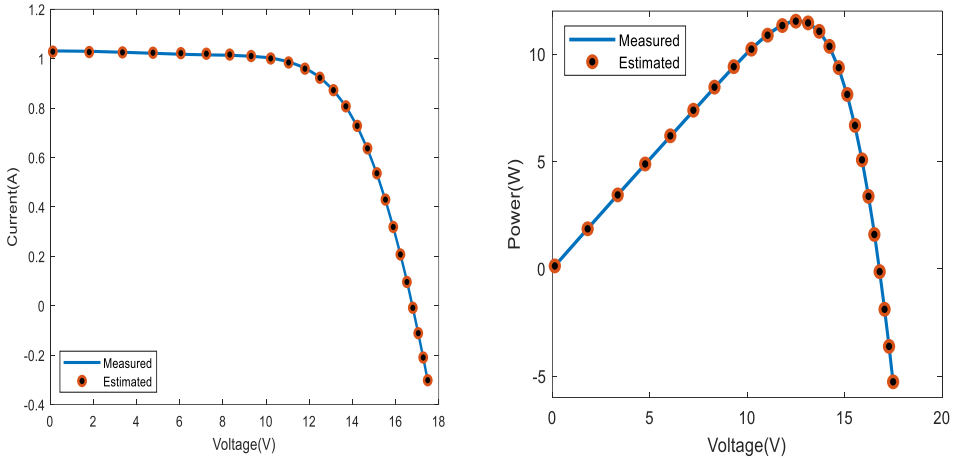

(a) **(b)**

Figure 17. Comparison of PMM. **(a)** I-V characteristics; **(b)** P-V characteristics.

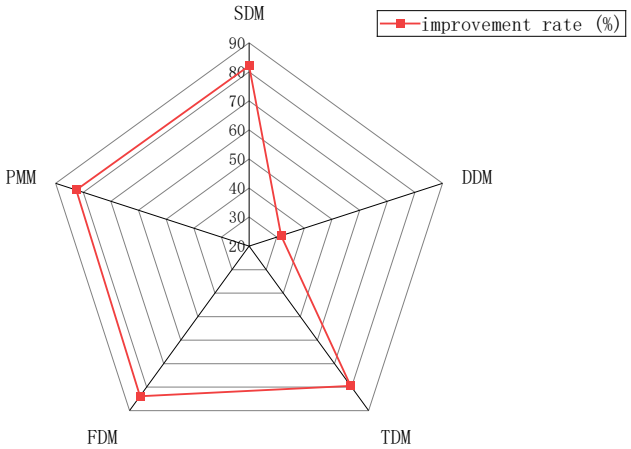

Figure 18. IRTH improvement rate radar chart.

This article calculates the δ_{mean} value of other algorithms, compares it with IRTH, calculates the model improvement rate, and presents the results in **Figure 18**. IRTH has been improved on different models. Among them, FDM and PMM have the highest improvement rates, reaching 83.89% and 82.56% respectively, while DDM

has a relatively low improvement rate, with an average improvement rate of 79.94%. This indicates that IRTH not only has significant improvement effects on individual models, but also has obvious overall advantages on all models. To ensure that the PV models (SDM, DDM, TDM) accurately represent real-world systems, the study further conducted an extensive data collection effort. PV system performance data were collected from different geographical locations and climatic conditions including various light intensity, temperature and load conditions. These included temperatures of 25 ℃, 30 ℃, 35 ℃ and light intensities of 800 W/m^2, 1000 W/m^2, 1200 W/m^2. Meanwhile, based on the manufacturer's data, the relevant parameters were initially estimated. The model calibration results were obtained, as shown in **Table 2**.

Table 2. Testing of model calibration results.

Temperature (℃)	Light intensity (W/m^2)	Actual voltage (V)	Model predicted voltage (V)
25	800	0.705	0.698
	1000	0.752	0.746
	1200	0.815	0.808
30	800	0.723	0.717
	1000	0.780	0.772
	1200	0.840	0.835
35	800	0.735	0.728
	1000	0.795	0.790
	1200	0.855	0.853

As can be seen from **Table 2**, the error between the model prediction results and the real voltage is small, with the error ranging from 0.004–0.008 V. This indicates that the over-calibrated model is able to predict the voltage output of the PV system under different conditions more accurately. It also shows that the robustness of the model is more reliable.

5. Cross-cutting applicability analysis

Finally, to further demonstrate the effectiveness of the IRTH algorithm, the study applies it to a logistics optimisation problem for algorithm performance evaluation. The Vehicle Routing Problem (VRP) is chosen as a test case. VRP is a classical problem in logistics and supply chain management, where the objective is to minimise the total distance travelled by a group of vehicles while satisfying customer demand and vehicle capacity constraints. In order to adapt the characteristics of VRP, the IRTH algorithm is first adapted. The population size and the number of iterations of the IRTH algorithm are adjusted, and the paths in the VRP problem are represented as a series of arrangements of customer nodes. Meanwhile, other heuristic algorithms are introduced to compare the performance of different methods in solving VRP. These include Genetic Algorithm (GA), Particle Swarm Optimisation (PSO) algorithm and Ant Colony Optimisation ACO) algorithm. A publicly available library of VRP instances, including test cases of different sizes (20, 50, and 100 client points) and different densities (sparse, medium, and dense) are selected for the experiments, and the specific results are shown in **Table 3**.

Table 3. Comparison results of different algorithms for solving VRP.

Algorithm	Mean number of convergences (Times)	Mean total distance travelled (km)	Mean completion time (s)	Standard deviation of total distance travelled (km)
IRTH	78	562.3	0.9	15.2
GA	120	588.7	1.2	22.6
PSO	95	575.4	1.1	18.4
ACO	105	581.9	1.2	20.1

As can be seen from **Table 3**, the IRTH algorithm proposed in the study is still superior in solving the VRP problem. Compared with GA, PSO and ACO, the average number of convergences of IRTH algorithm is reduced by 35%, 17.89% and 25.71% respectively. Comparing the average total distance travelled by the vehicles under the four algorithms, it can be seen that the IRTH solution is more advantageous, with the logistics vehicle travelling a distance of only 562.3 km, and the completion time of the solution is only 0.9 s. This indicates that the IRTH algorithm has a faster convergence speed, higher solution quality and good robustness in solving the VRP problem. Compared with other heuristic algorithms, the IRTH algorithm provides better solutions in most cases. These results further demonstrate the flexibility and powerful optimisation capabilities of the IRTH algorithm.

6. Conclusion

This article proposed an IRTH algorithm for photovoltaic cell PI, which effectively improved the precision and velocity of photovoltaic cell model PI. The specific summary is as follows:

(1) Multiple mathematical models of DDM and photovoltaic modules were constructed, and objective functions and solution vector models were established based on them. Subsequently, the key parameters to be identified in each model were identified, and RMSE was used as the standard to measure the accuracy of PI.

(2) Multidimensional improvements have been made to the RTH to avoid being FILO, and to enhance the original algorithm's global search ability and convergence velocity.

(3) Innovatively analogizing the photoelectric conversion unit to a biomaterial unit with specific mechanical response characteristics, and deeply exploring the current voltage characteristics of photovoltaic cells from the perspective of mechanical response characteristics.

(4) The improved RTH was taken to make PI of the photovoltaic cell model. The optimal and average values were superior to other models, with an average improvement rate of 79.94%.

The PI method for photovoltaic cells grounded on IRTH presented in this article mainly aims to achieve PI for five typical photovoltaic models. The next step will be to study the fault diagnosis method for photovoltaic cells.

Author contributions: Conceptualization, ZY and YZ; methodology, YS; software, YZ; validation, CG, YS and XD; formal analysis, YZ; investigation, ZY; resources, CG; data curation, YS; writing—original draft preparation, YZ; writing—review and

editing, ZY; visualization, XD; supervision, YS; project administration, CG; funding acquisition, ZY. All authors have read and agreed to the published version of the manuscript.

Funding: This work was supported by National Natural Science Foundation of China (52307204).

Ethical approval: Not applicable.

Conflict of interest: The authors declare no conflict of interest.

References

1. Minhong L, Guanxin Q, Yong Z, et al. Research on centralized access of photovoltaic inverters to active distribution network based on two-stage robust optimal scheduling. Electrical Measurement & Instrumentation, 2024, 61(9).
2. Drif M, Bouchelaghem A, Guemache A, et al. A Novel Method to Obtain Reverse Bias I–V Curves for Single Cells Integrated in Photovoltaic Modules. Power Electronics and Drives, 2024, 9(1):412-427.
3. Pietrzak P, Wolkiewicz M. Condition Monitoring and Fault Diagnosis of Permanent Magnet Synchronous Motor Stator Winding Using the Continuous Wavelet Transform and Machine Learning. Power Electronics and Drives, 2024, 9(1):106-121.
4. Jinkun L, Fazhi H, Xiaoxin G. An enhanced grey wolf optimizer with fusion strategies for identifying the parameters of photovoltaic models. Integrated Computer-Aided Engineering,2022,30(1):89-104.
5. Chen H, Jiao S, Heidari A A, et al. An opposition-based sine cosine approach with local search for parameter estimation of photovoltaic models. Energy Conversion and Management,2019,195927-942.
6. Xiaojia Y, Wei L, Hong L, et al. Modified Whale Optimization Algorithm for Solar Cell and PV Module Parameter Identification. COMPLEXITY,2021.
7. Wang P, Yang Q, Liu Y, et al. Design and simulation experiment of photovoltaic power generation systems for zero-energy solar houses. Experimental Technology and Management, 2024, 41(7):103-111.
8. Ferahtia S, Houari A, Rezk H, et al. Red-tailed hawk algorithm for numerical optimization and real-world problems. Scientific Reports, 2023, 13(1): 12950.
9. Alshahrani H J, Hassan A Q A, Almalki N S, et al. Applied Linguistics With Red-Tailed Hawk Optimizer-Based Ensemble Learning Strategy in Natural Language Processing. IEEE Access, vol. 11, 2023:132448-132456.
10. Gong B, An A, Shi Y, et al. Fault diagnosis of photovoltaic array with multi-module fusion under hyperparameter optimization. Energy Conversion and Management, 2024, 319.
11. Mohamed Abdel-Basset, Doaa El-Shahat, Ripon K, et al. Parameter estimation of photovoltaic models using an improved marine predators algorithm, Energy Conversion and Management, Volume 227,2021,113491.
12. Fan G F, Li J W, Peng L L, et al. The bi-long short-term memory based on multiscale and mesoscale feature extraction for electric load forecasting. Applied Soft Computing, 2024, 162.
13. Al-Ani M A J, Zdiri M A, Salem F B, et al. Optimized Grid-Connected Hybrid Renewable Energy Power Generation: A Comprehensive Analysis of Photovoltaic, Wind, and Fuel Cell Systems. Engineering, Technology & Applied Science Research, 2024, 14(3).
14. Bai W, Zhang Z, Zhang Y, et al. Virtual coupling control of photovoltaic-energy storage power generation system for efficient power support. Energy Reports, 2024, 12:1742-1752.
15. Changting Z, Gang L, Zeng M. Beluga whale optimization: A novel nature-inspired metaheuristic algorithm. Knowledge-Based Systems, 2022, 251.
16. Su H, Zhao D, Heidari A A, et al. RIME: A physics-based optimization. Neurocomputing, 2023, 532: 183-214.
17. Deng L, Liu S. Snow ablation optimizer: A novel metaheuristic technique for numerical optimization and engineering design. Expert Systems with Applications, 2023, 225: 120069.
18. Wang R, Liu H, Zhang Y, et al. Integrated photovoltaic charging and energy storage systems: mechanism, optimization, and future. Small, 2022, 18(31): 2203014.
19. Meng J, Sun Y, Wang Y, et al. Cooperative adaptive inertial control for PV and energy storage units with multiple constraints. IET Renewable Power Generation, 2022, 16(10): 2076-2087.

20. Bencherif M, Brahmi N. Solar cell parameter identification using the three main points of the current–voltage characteristic. International Journal of Ambient Energy, 2022, 43(1): 3064-3084.
21. Almousa M T, Gomaa M R, Ghasemi M, et al. Single-Sensor Global MPPT for PV System Interconnected with DC Link Using Recent Red-Tailed Hawk Algorithm. Energies, 2024, 17(14): 3391.
22. Qian P, Pu C, Liu L, et al. Ultra-high-precision pneumatic force servo system based on a novel improved particle swarm optimization algorithm integrating Gaussian mutation and fuzzy theory. ISA transactions, 2024, 152: 453-466.
23. Shishavan S T, Gharehchopogh F S. An improved cuckoo search optimization algorithm with genetic algorithm for community detection in complex networks. Multimedia Tools and Applications, 2022, 81(18): 25205-25231.
24. Anand K, Vijayaraj A, Vijay Anand M. Privacy preserving framework using Gaussian mutation based firebug optimization in cloud computing. The Journal of Supercomputing, 2022, 78(7): 9414-9437.
25. Aziz R M. Cuckoo search-based optimization for cancer classification: A new hybrid approach. Journal of Computational Biology, 2022, 29(6): 565-584.
26. Layeb A. Tangent search algorithm for solving optimization problems. Neural Computing and Applications, 2022, 34(11): 8853-8884.